Three-point bending performance of sandwich panels with various types of cores

Fukun Xia[1], Yvonne Durandet[1], PJ Tan[2] and Dong Ruan[1]*

[1]Department of Mechanical and Product Design Engineering, School of Engineering,

Swinburne University of Technology, Hawthorn, VIC3122, Australia

[2]Department of Mechanical Engineering, University College London, Torrington Place,

London WC1E 7JE, UK

*Corresponding author. druan@swin.edu.au

ABSTRACT

In this paper, the bending performances of sandwich panels with corrugated triangular, honeycomb, aluminium foam, pyramidal truss, double sine corrugated (DSC), and 3D re-entrant auxetic cores are assessed and compared, both experimentally and numerically. Three-point bending experiments were performed on corrugated, honeycomb, aluminium foam, and truss core sandwich panels with identical face-sheets and core height. The experimental and numerical results compared well for panels with corrugated, honeycomb and truss cores. Parametric studies were subsequently performed, using ABAQUS, and three distinct modes of deformation were identified. The specific energy absorption (SEA) of the panels was found to increase with the core relative density; the one with a honeycomb core will be shown to have the greatest SEA, for the same core relative density, compared to the rests.

KEYWORDS

Corrugated sandwich panel; honeycomb; aluminum foam; truss sandwich panel; auxetics; bio-inspired structure.

1. INTRODUCTION

Sandwich panels consisting of a low-density core and thin skins (upper and lower) are widely used in applications that require a combination of high structural rigidity and lightweight, such as in aerospace, ships, and railway industry [1–4]. A sandwich panel construction offers higher specific stiffness and strength to weight ratio compared to its monolithic counterpart. Corrugated and truss structures, honeycombs and metal foams are often used in sandwich cores [5]. The different core materials/types are briefly reviewed below.

Metal foams, also known as stochastic foams (manufactured using a foaming route), can generally be classified as open or closed-cell (where the cells are enclosed within cell walls). The strength of metal foam is related to its relative density through a power-law relationship [6]. An advantage of metal foam is that they have nearly isotropic mechanical properties. A metal foam core sandwich panel typically fails by face yielding, face wrinkling, core yielding, or local indentation [7]. Crupi et al. [8] observed different modes of deformation under three-point bending which depends on the support span distance and the foam properties.

A common feature of a prismatic honeycomb structure is its array of prismatic hollow cells separated by thin vertical walls. The cell geometry varies widely, and the common ones are hexagonal [9], columnar [10], and square [11,12]. A honeycomb structure exhibits high out-of-plane compressive strength and shear properties, compared to its in-plane counterpart, at low density [13]. In most of the honeycomb sandwich structures, the axes of the prismatic core cells are perpendicular to the face-sheets. The failure mechanisms that develop under three-point bending include core shear, face yielding, face bending, indentation, and face wrinkling [14–17]. Crupi et al. [16] altered the span of the support rollers and reported two different deformation modes. Sun et al. [17] showed that the deformation mode is affected by the geometric parameters of the honeycomb panels. The diameter of the loading pin was also found to influence the deformation mode [10]. An increase in the roller diameter leads to a

larger deformation zone. With a smaller roller diameter, localised indentation is the dominant deformation mode due to fewer core cells underneath the indenter. By contrast, the deformation mode for a larger roller diameter is core shear together in combination with face-sheet bending.

A truss core comprises of struts organized into interconnected triangle units. The interior structure of a truss sandwich panel facilitates its multifunctional (e.g., crossflow heat exchange and shape morphing) applications [18]. Deshpande et al. [19] identified four competing failure mechanisms, viz. face yielding, face wrinkling, indentation, and core shear, where failure maps were constructed. Xiong et al. [20] investigated the bending performance of sandwich panels with pyramidal truss cores and carbon fiber composite face-sheets, where the failure mechanisms observed were face sheet crushing, face sheet wrinkling, core member buckling, and core crushing.

A corrugated core comprises of corrugated plates or sheets that can be triangular, trapezoidal, or curvilinear [21–24]. Corrugated sandwich panels are often preferred in many applications since they are easy to manufacture, typically through a welding route [25]. However, their bending performances vary according to the loading direction due to anisotropy. Depending on the loading direction relative to the axis of the corrugated core, bending tests can be performed along the two principal directions as shown schematically in Fig. 1: transverse (i.e., bending about an axis perpendicular to the corrugation axis) and longitudinal (i.e., bending about an axis parallel to the corrugation axis). Lu et al. [26] identified four failure mechanisms (i.e., face yielding, core yielding, face buckling, and core buckling) and derived failure criterion for the triangular corrugated sandwich panels under bending. Based on the work from Lu et al [26], Valdevit et al. [27,28] constructed failure maps for simply supported triangular corrugated sandwich beams subjected to transverse and longitudinal three-point bending.

Bio-inspired structures have great potential as energy absorbers. For example, Odontodactylus scyllarus, commonly known as the peacock mantis shrimp, uses its dactyls to smash through mollusk shells and other tough mineralized structures with tremendous force and speed. The dactyls can withstand repetitive impact forces up to 1.5 kN [29]. The pitch-graded sinusoidal herringbone pattern in the dactyl helps to achieve this remarkable property. Yang et al. [30] studied the uniaxial compression response of a sandwich panel whose double-sine corrugated core was arranged in a bio-inspired sinusoidal herringbone pattern. The sandwich panel with double-sine corrugated core was found to have greater energy absorption capacity and smaller initial peak force compared with triangular corrugated core sandwich panel.

Auxetic materials/structures exhibit negative Poisson's ratios and have excellent mechanical properties such as enhanced indentation resistance and energy absorption ability [31]. A 3D re-entrant auxetic structure is extended from a 2D re-entrant hexagonal honeycomb structure and exhibits auxetic behavior in all three principal directions. Wang et al. [31] and Yang et al. [32] proposed analytical models for the modulus, Poisson's ratio and yield strength of the 3D re-entrant structures. Chen et al. [33] has used auxetic structures as core of sandwich panel to study its blast response. The panel with auxetic core outperformed the one with hexagonal honeycomb core when the blast level was low, or the core relative density was high.

Hitherto, there are relatively few attempts to compare the bending performance of sandwich panels with different core types. Results from three-point bending experiments of sandwich panels with corrugated, truss, honeycomb and foam cores will be reported and their performance (specific energy absorption) quantified and compared. Numerical models are developed, where their predictions were validated by the experimental data, and the former is used in a parametric study to elucidate the load-displacement curves and modes of deformation

4

that develop during bending. Finally, their specific energy absorptions are quantified and compared.

2. EXPERIMENTS

2.1 Samples

The sandwich panels were manufactured by adhesively bonding two Al5005-H34 face-sheets to various core materials/types using Araldite 420 A/B epoxy adhesive. Subsequently, the samples were cured at 70 °C for two hours. All the samples have identical x-z plane dimensions of 200 mm $\times$ 50 mm, with an identical face-sheets thickness (t_f) of 1.0 mm and a core height (h_c) of 12.5 mm. Four types of sandwich core materials/types were investigated, viz. triangular corrugated, pyramidal truss, honeycomb, and aluminum foam.

The triangular corrugated core was fabricated by moulding an Al5005-H34 sheet into corrugations. Fig. 1 (a) shows the longitudinal and transverse orientations of a corrugated sandwich panel, respectively. The two key geometric parameters of the corrugations are the web thickness, t_c, and corrugation angle, θ_c. Fig. 1 (b) shows the schematic of a pyramidal truss core sandwich panel with strut thickness, t_t, strut width, w_t, and strut angle, θ_t (the angle between the strut and the lower face sheet). A water jet was used to generate a two-dimensional periodic diamond pattern from an Al5005-H34 sheet, which was subsequently moulded into the required shape as shown in Fig. 2. The honeycomb core was made from Al5052, where d_h and t_h are the cell size and cell wall thickness, respectively, as shown in Fig. 1 (c). Fig. 1 (d) shows an aluminum foam core sandwich panel, where the core was machined from a block of ALPORAS aluminum foam with a relative density ($\bar{\rho}$) of approximately 8%. Table 1 lists the geometric parameters, mass and material types for the different sandwich panels to be investigated here. Eight types of sandwich core, viz. Corrugated-T, Corrugated-L, Truss-A, Truss-B, Honeycomb-A, Honeycomb-B, Honeycomb-C, and Foam, were used experimentally.

The geometric configuration and dimensions for each are listed in Table 1. Three samples of each type were fabricated and tested.
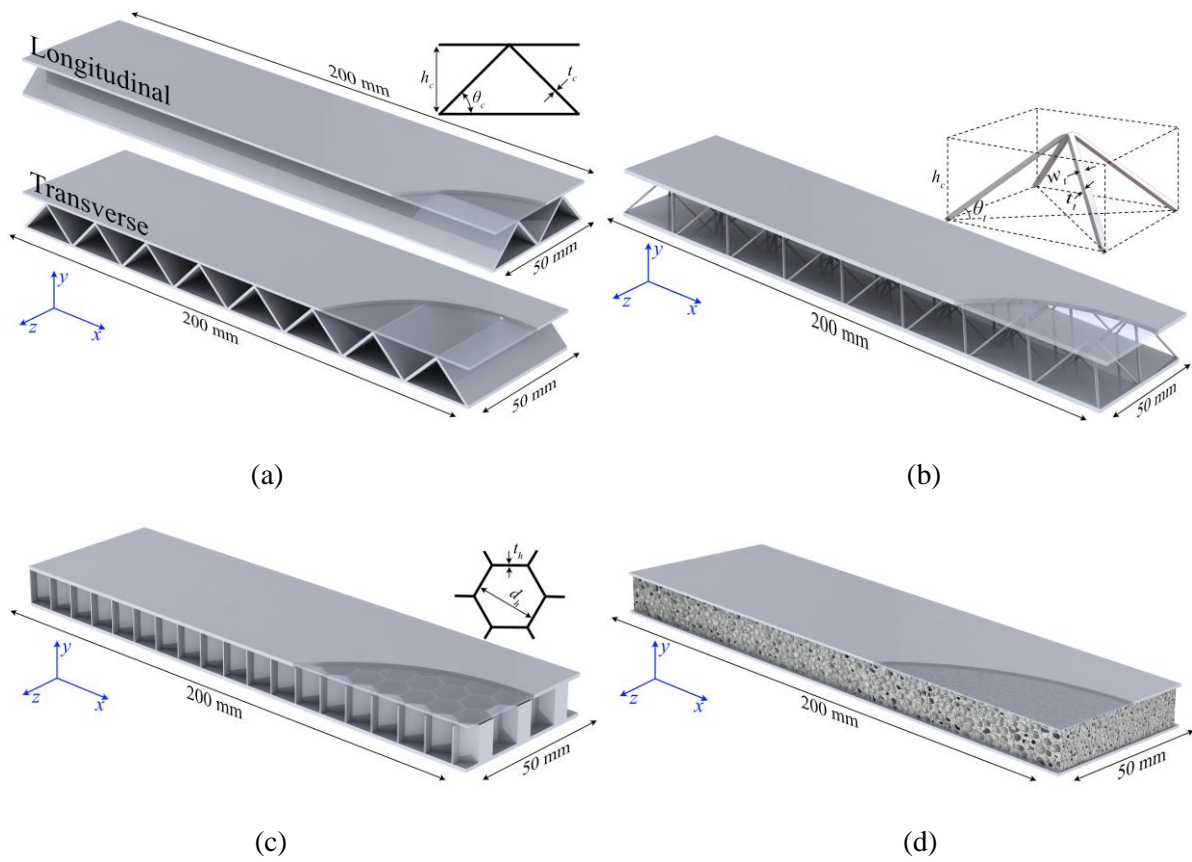

(a) (b)

(c) (d)

Fig. 1. Schematics of the sandwich panel with (a) corrugated, (b) truss, (c) honeycomb, and (d) aluminium foam cores.
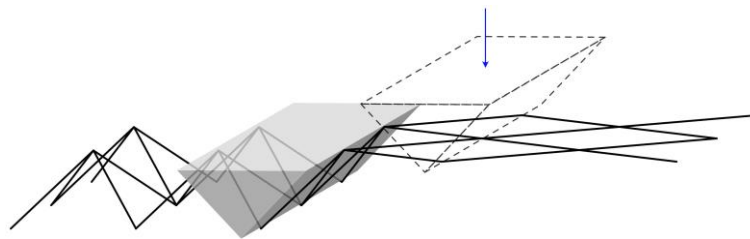

Fig. 2. Forming the pyramidal truss core.

Table 1. Geometric configuration and dimensions of the sandwich panels

Sample	Orientation	t_c (mm)	θ_c (°)	Core material	Average mass (g)
Corrugated-T	Transverse	1.0	45	Al5005-H34	95.0
Corrugated-L	Longitudinal	1.0	45	Al5005-H34	95.3

	w_t (mm)	t_t (mm)	θ_t (°)		
Truss-A	2.0	0.6	35.26	Al5005-H34	59.7
Truss-B	2.0	1.0	35.26	Al5005-H34	62.7
	d_h (mm)	t_h (mm)			
Honeycomb-A	3.18	0.0254		Al5052	66.7
Honeycomb-B	3.97	0.0381		Al5052	67.7
Honeycomb-C	6.35	0.0762		Al5052	71.0
	$\bar{\rho}$				
Foam	8%			Al-Ca5-Ti3 [34]	86.1

2.2 Mechanical properties of face-sheets and core

Aluminum (Al5052-H34) sheets with thicknesses of 0.6 mm and 1.0 mm were used in the fabrication of the truss core and face-sheets, respectively. Five dog-bone-shaped tensile coupons were machined from each sheet thickness, and uniaxial tensile tests were performed to obtain the material properties of Al5052-H34 in accordance with the ASTM standard E8/E8M-15a. The tensile true stress-strain curves are plotted in Fig. 3. The average Young's modulus and yield strength for the 0.6 mm and 1.0 mm sheet are 52.1 GPa and 112.3 MPa, and 53.5 GPa and 114.0 MPa, respectively.

The material properties for the Al5052 alloy that was used to manufacture the honeycomb core are listed in Table 2. ALPORAS foams with an out-of-plane dimension of 50 mm × 50 mm and a height of 12.5 mm were cut from a large foam block. The foams were compressed uniaxially at a rate of 2 mm/min, and the tests were repeated three times - the compressive stress-strain curves are shown in Fig. 4.
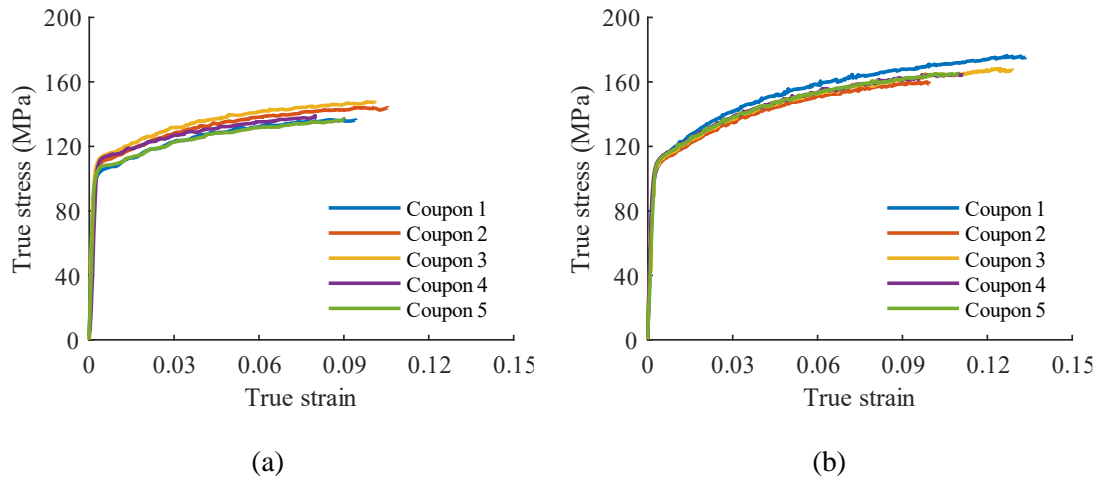
Fig. 3. True stress-strain curves of the tensile coupons from the (a) 0.6 mm and (b) 1.0 mm thick aluminum sheets.

Table 2. Material parameters for Al5052 aluminum alloy [35] (parameters listed were those used in the Johnson-Cook constitutive model in subsequent finite element simulations.)

E (MPa)	ν	A (MPa)	B (MPa)	n	$\dot{\varepsilon}_0$ (s^{-1})	C	m	T_{melt} (K)	T_0 (K)
73000	0.33	256	426	0.34	1	0.015	1	823	273
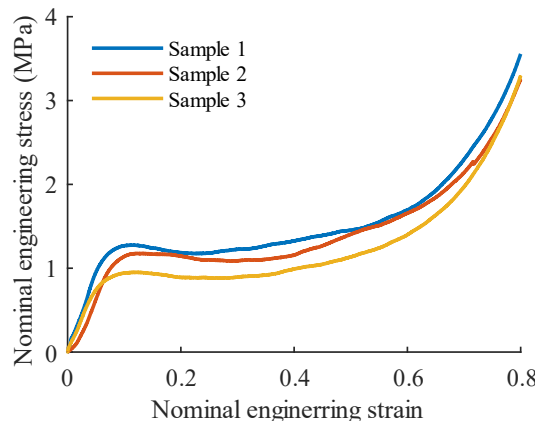
Fig. 4. Compressive stress-strain curves of ALPORAS foam with a relative density of approximately 8%.

2.3. Three-point bending tests

Three-point bending experiments were performed on a 50 kN MTS machine (model 43) using a bending fixture (model FWA105A) at a loading rate of 1.5 mm/min. Three repeat tests were performed for each sandwich panel with a different core material/type. The loading pin/indenter and support rollers were made of high strength steel and had a diameter of 20 mm. The span between the two support rollers is $l = 150$ mm. For sandwich panels with a corrugated-T and truss-A and Truss-B core, the indenter was placed at the mid-point between two vertices, as shown in Fig. 5.

(a)

(b)
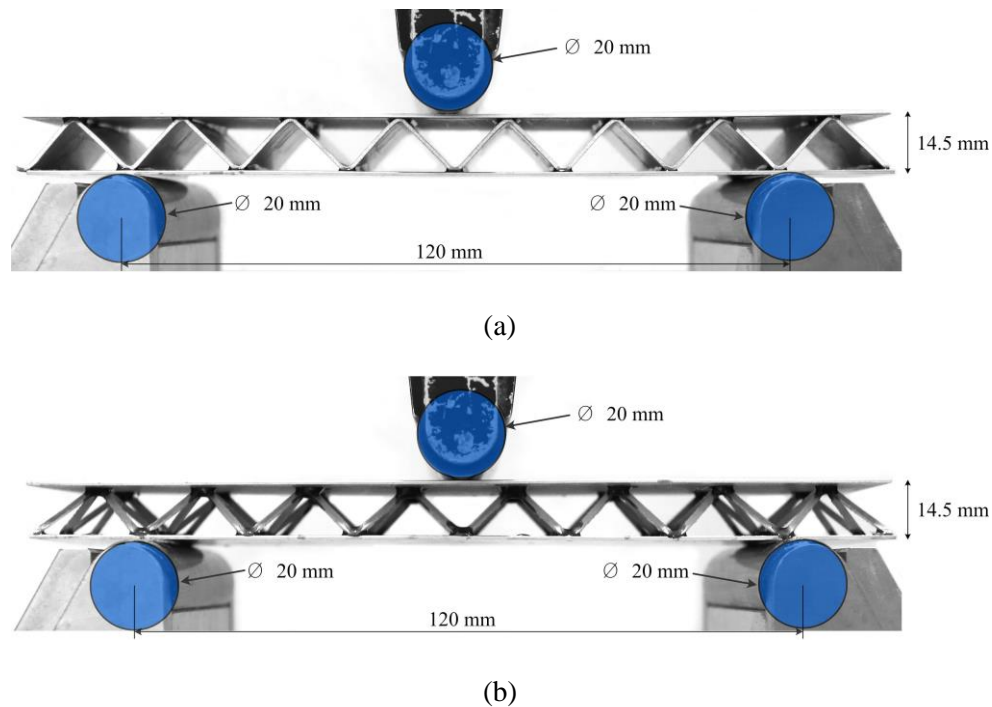
Fig. 5. Three-point bending experimental setup for sandwich panels with (a) corrugated-T and (b) truss-A cores.

3. FINITE ELEMENT ANALYSIS (FEA)

Finite element (FE) simulations were performed using ABAQUS/Explicit. Panels with five different types of core materials/types were simulated: triangular corrugated core, pyramidal truss core, honeycomb core, double sine corrugated core (DSC), and 3D re-entrant

auxetic core. However, the aluminum foam-core sandwich panel was not simulated in the parametric study due to a lack of precise material properties (such as failure strain) for different relative densities.

The material properties for Al5005-H34, see Section 2.2, were used in the FE models of the face-sheets and cores (corrugated and truss). The Johnson-Cook constitutive model was used to simulate the cell wall material of the honeycomb core - see Table 2. Although the face-sheets and cores were bonded adhesively in the experiments, the adhesive layer was not considered in the simulations. Since no debonding was observed in the experiments, perfect bonding between the face-sheets and core was assumed in all the FE models by tying the cores to the face sheets. General contact, with a friction coefficient of 0.2, between the indenter/support rollers with the face sheets was used. Both support rollers and the indenter were assumed to be rigid bodies. All degrees of freedom for the two support rollers were fixed, and the indenter is displaced in z-direction at a constant displacement rate of 50 mm/s – note that this is higher than in experiments - to reduce the computational time. Our previous study [37] have already shown that dynamic effects are negligible up to a loading rate of 50 mm/s. Four-node shell elements (S4R) were used to mesh the face-sheets of the sandwich panels, including for the corrugated and honeycomb cores. The truss core and the rollers were meshed by two-node linear beam elements (B31) and four-node rigid elements (R3D4), respectively. Convergence study has shown that a mesh size of 1 mm for the corrugated and truss sandwich panel, and 0.5 mm for the honeycomb core is sufficient to give accurate results.

4. RESULTS AND DISCUSSIONS

4.1 Experimental and FE results
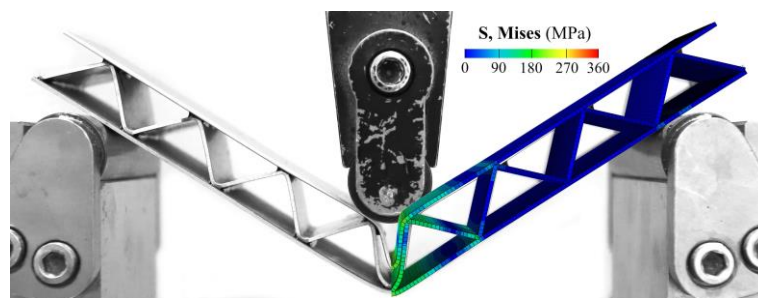
4.1.1 Corrugated core panel

Since the deformation mode observed in each repeated test is largely identical, only one representative test result for the Corrugated-L and Corrugated-T panels is shown in Fig. 6 (a) and (b), respectively. The images on the left are from experiments and those on the right are numerical predictions. In general, the FE simulations can capture well the deformation modes observed in experiments. Global bending and local indentation (beneath the indenter) were observed in both the Corrugated-L and Corrugated-T panels. In the Corrugated-L panel, the corrugated core underneath the indenter deforms locally by bending from interactions with the top face-sheet that intrudes into the core space. By contrast, the top face-sheet of the Corrugated-T panel intrudes into the void space of the corrugations along the y-direction, leading to a somewhat more localised indentation compared to its Corrugated-L counterpart – compare Fig 6(a) and (b).

The load-displacement curves of the corrugated sandwich panels subjected to transverse and longitudinal bending are shown in Fig. 6 (c) and (d), respectively. The peak load of a Corrugated-L panel is approximately six times higher than its Corrugated-T counterpart. This is unsurprising since, in the former, the intrusion by the top face sheet is resisted by all the corrugations along the x-direction, unlike the latter. In general, the FE model successfully captures the general trend of the load-displacement curve obtained experimentally. For the Corrugated-T panels, the peak load initially reaches ~0.5 kN, in both the experiments and simulations, then drops and increases again to a secondary peak reaching, on average, 0.43 kN in the experiments and 0.52 kN in the simulations. The secondary peak occurs when the indenter comes into further contact with parts of the top face-sheet where its underlying
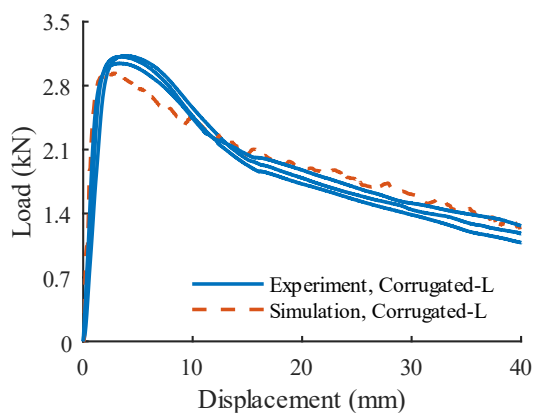
corrugations are not yet deformed. The load fluctuations and higher second peak load in the FE simulations are caused by the unstable contact conditions in the deformation process.
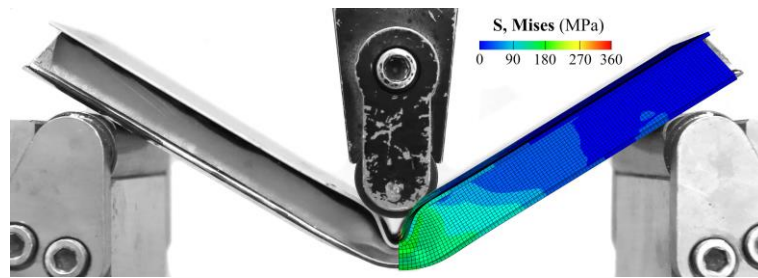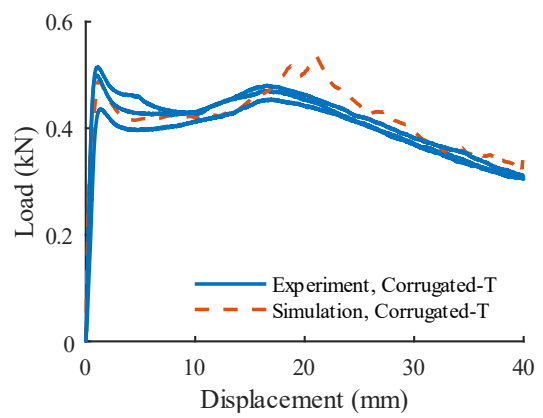

(a)

(b)

(c)

(d)

Fig. 6. Comparison between experimental and numerical results: (a) Corrugated-L panel; (b) Corrugated-T panel; (c) load-displacement curves of Corrugated-L panels; and, (d) load-displacement curves of Corrugated-T panels.

4.1.2 Truss core panel

Two deformation modes were observed for the Truss-A panel. As shown in Fig. 7 (a), all the core struts on the left side of the panel had collapsed. By contrast, this only occurred for those core struts next to the indenter on the right. This asymmetric deformation was induced because the indenter was not positioned exactly at the mid-point of the panel in the experiments - the offset was approximately 1 mm. The FE simulation (Simulation 1) also predicts an asymmetric deformation when the indenter is positioned by a similar offset from the mid-point. Figure 7(b) shows a Truss-A panel that deformed symmetrically when indenter is placed at the mid-point of the panel – this was observed both in the experiments and FE simulation (Simulation 2). The top face-sheet intrudes into the core space, crushing the two core cells immediately beneath the indenter, and almost came into contact with the bottom face-sheet at the end of the crushing process. Fig. 7 (c) shows that a Truss-B panel exhibits similar symmetric deformation to that of Truss-A. However, the region of local indentation is smaller in Truss-B due to its stronger core (higher t_t).

Three experimental and two FE-predicted load-displacement curves are plotted in Fig. 7 (d) for the Truss-A panel. The peak load in both experiments and numerical predictions are approximately 0.35 kN. The average load after the indenter displacement of 10 mm in simulations is approximately 0.15 kN – this is slightly higher than those in experiments (0.12 kN). If there is offset of the indenter, two of the experimental curves and the curve of Simulation 1 fluctuate severely until the indenter displacement reaches approximately 10 mm – this is due to the collapse of the core cells on the left side of the panel. By contrast, the curves (obtained from experiment and simulation) without offset of the indenter is less than 5 mm, which corresponds to the collapse of the two cells beneath the indenter.

The load-displacement curve of the Truss-B panel showed less fluctuations. The thicker core struts provide stronger support to the face-sheets. In one of the experiments, the load drops

abruptly at a displacement of 16 mm due to the debonding in the panel. In these two experiments (no debonding occurred), the top face-sheets came into contact with the adhesive on the bottom face-sheet at the indenter displacement of 30 mm, after which the force increased. The simulated load has a similar peak and overall trend. However, the higher simulated load when the indenter displacement is from 10 mm to 20 mm and the lower simulated one after the indenter displacement of 30 mm may be caused by the manufacturing error and adhesive.

(a)

(b)

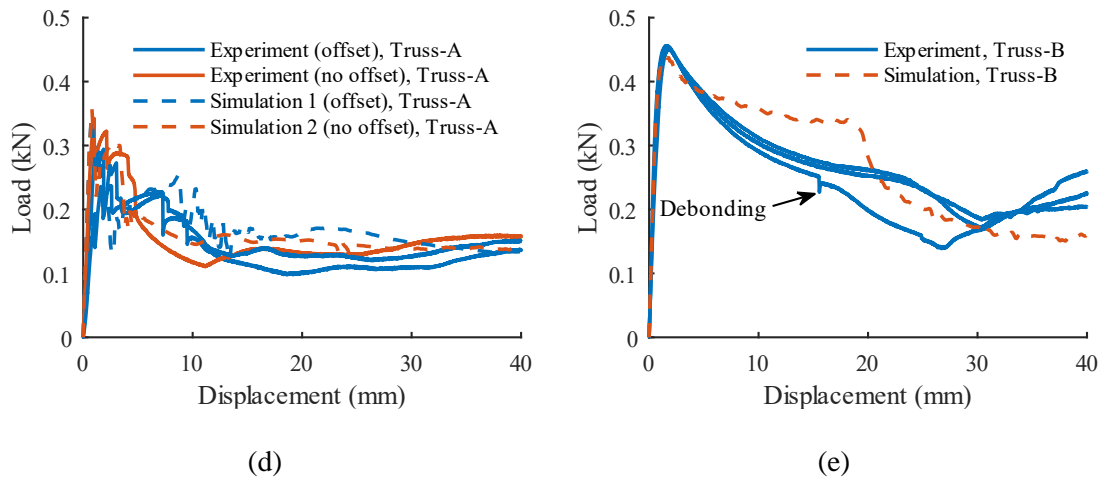(c)

(d)   (e)
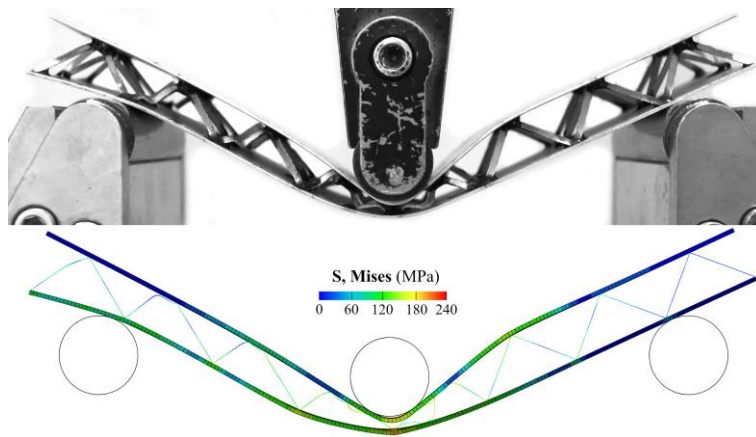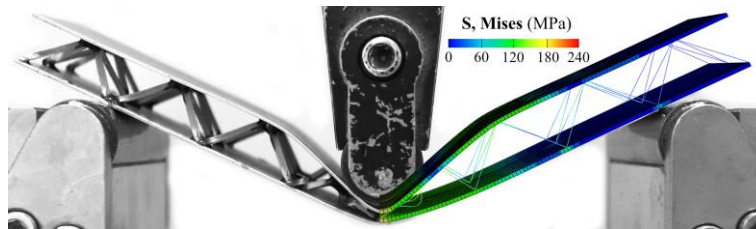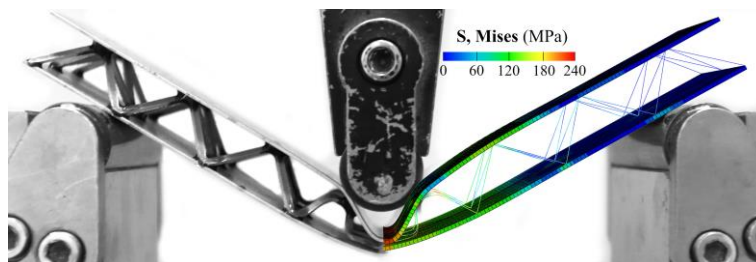
Fig. 7. Comparison between experimental and numerical results: (a) Truss-A panel when indenter was 1 mm away from the middle of the panel; (b) Truss-A panel when the indenter was in the middle of the panel; (c) Truss-B panel; (d) load-displacement curves of samples Truss-A panels; and, (e) load-displacement curves of samples Truss-B.

4.1.3 Honeycomb core panel

Honeycomb-A, Honeycomb-B, and Honeycomb-C have a similar deformation mode – global bending along with a narrow region of deep local indentation – which is seen in both experiments and FE simulations (see Fig. 8a-c). Only a very small portion of the core under the indenter was crushed. The same deformation mode was also reported in [16] and [17]. In the study of Sun et al. [17], the deformation mode shown in Figs. 8 (a)-(c) was denoted as Mode A, in which a void occurred underneath the indenter due to the deformation of the top face-sheet. In the other mode (Mode B), the indenter was in full contact with the deformed top face-sheet. The panels with thinner skin and greater honeycomb cell size tend to deform in Mode A

The predicted load-displacement curves (see Fig. 8d-e) by FE match reasonably well with their corresponding experimental one - the peak loads are 1.37 kN, 1.79 kN, and 2.10 kN. The differences of experimental and simulated loads in the initial stage maybe because of the

15

adhesive layer in experiments. The tie connection between the core and face-sheets in simulation was stronger than the adhesive bonding in experiments. Honeycomb-A has the lowest peak load (1.38 kN for both experiments and simulation) since it has the weakest core, followed by Honeycomb-B (1.81 kN for experiments and 1.62 kN for simulation) and Honeycomb-C (2.08 kN for experiments and 1.94 kN for simulation) whose core relative density is the highest of the three.
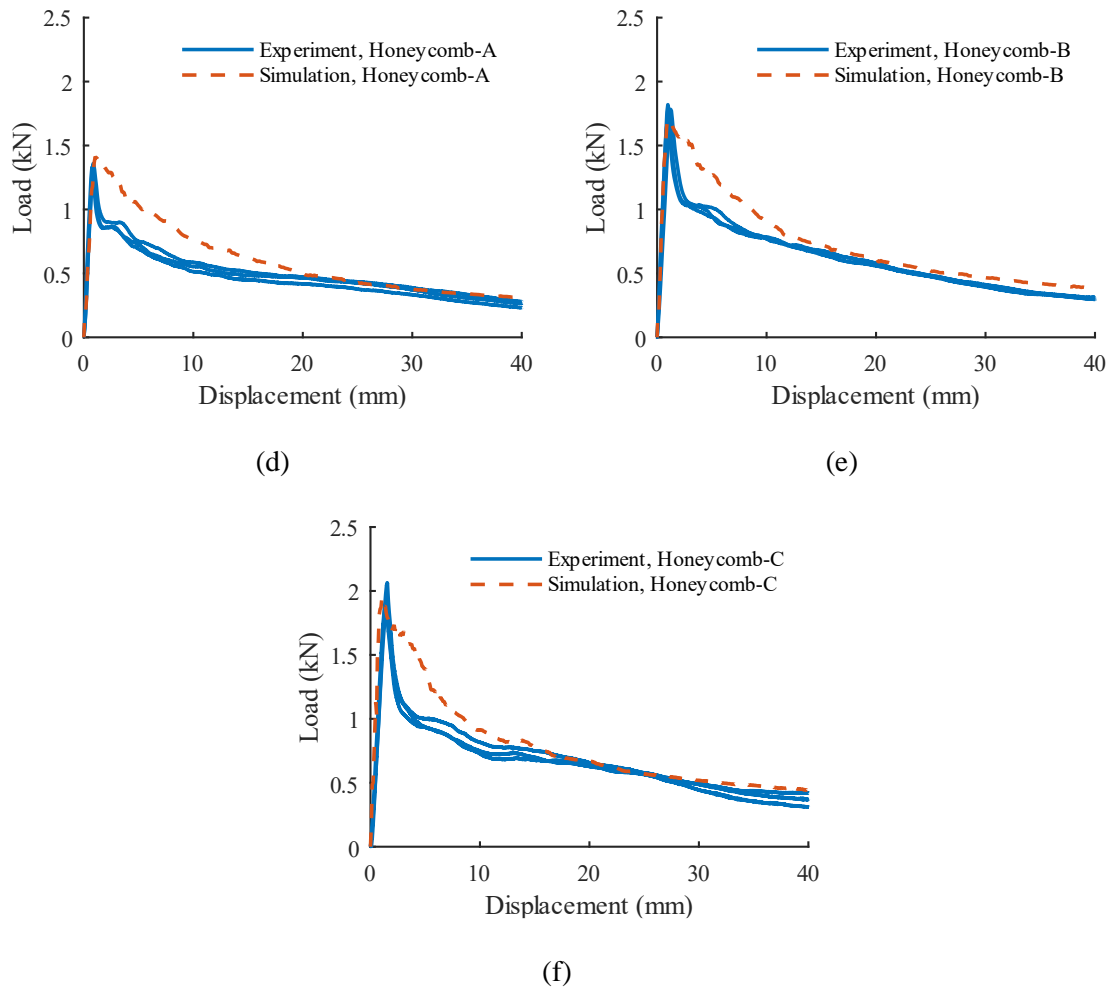

(a)

(b)

(c)

(d)

(e)

(f)
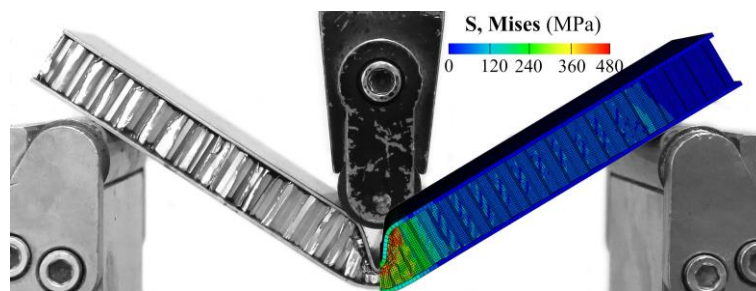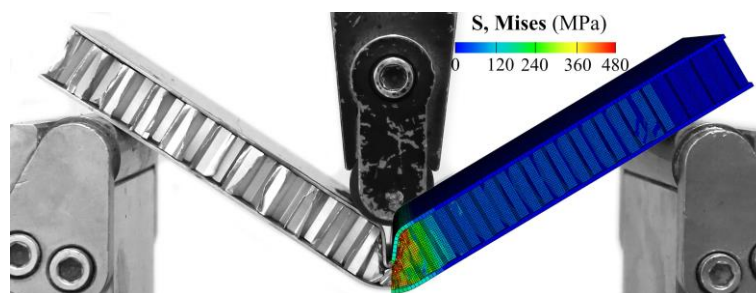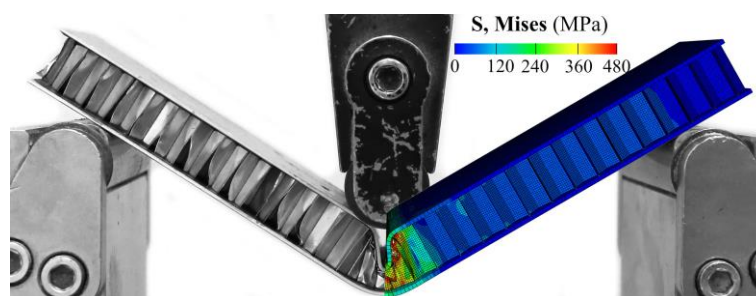
Fig. 8. (a), (b), and (c) are the experimental (left image) and numerical (right image) defrmation modes for Honeycomb-A, Honeycomb-B, and Honeycomb-C panels, respectively. Their corresponding load-displacement curves are shown in (d), (e), and (f), respectively.

4.1.4 Aluminum foam core panel

Core shear failure occurred in the foam core panels, as shown in Fig. 9 (a), (b), and (c). Plastic hinges developed along two sections of the panel – one beneath the indenter, and the other close to one of the supports (shown by the red dots in Fig. 9a). This asymmetric deformation mode is similar to Mode II deformation mode observed by Crupi et al. [8], which tends to occur in the experiments with the smaller span of supports. Fig. 9 (d) shows the load-

displacement curves of the panels. The sharp drops in the load-displacement curves are caused by the shear damage of the core (highlighted in the blue ovals).
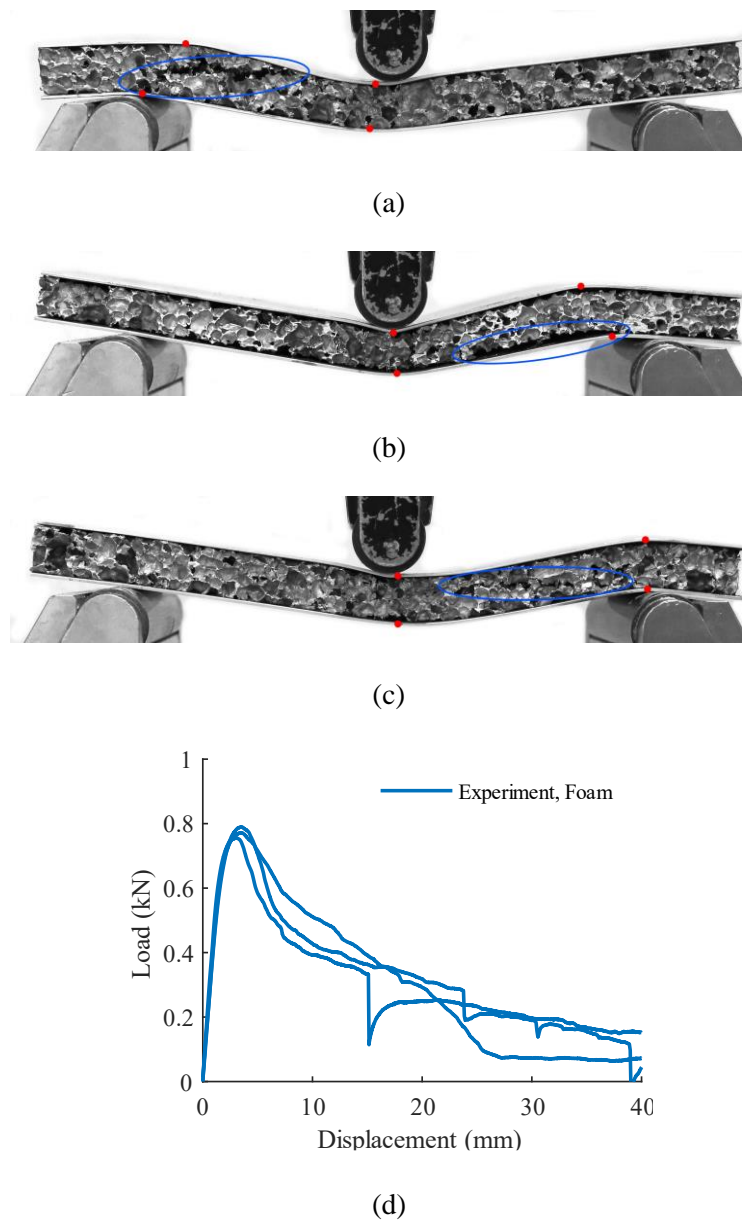

(a)

(b)

(c)

(d)

Fig. 9. Experimental results of aluminum foam sandwich panels: (a), (b), and (c) are the deformations of the panels when the indenter displacement is 10 mm; (d) load-displacement curves.

4.2 Parametric study

Figures 6, 7, and 8 show a good agreement between FE predictions and experimental results, both in terms of the deformation mode and load-displacement curve. The validated

numerical models are now employed to perform parametric study for the corrugated, truss and honeycomb core panels. In the parametric study, the core material and face-sheets are assumed to be made from Al5005-H34. Some of the geometric parameters for the panels are fixed, viz. face-sheet thickness is 1.0 mm, core height is 12.5 mm, the span between the two support pins is 150 mm, and the diameter of support pins and indenter is 20 mm. Aluminum foam sandwich panel is not considered due to a lack of an accurate material constitutive model.

For corrugated sandwich panels, the parametric study is conducted on panels subjected to both transverse and longitudinal bending. Under transverse bending, our previous work [36] showed that the position of the indenter affects the bending performance of a corrugated core panel. Two loading scenarios, viz. base indentation and node indentation, were investigated. The indenter was positioned at the mid-point between two vertices for base indentation and on top of the central vertex for node indentation. The peak load in node indentation is much higher than that in base indentation. Therefore, both node and base indentations will be considered here. Similar to the corrugated core panels, a truss core panel is also sensitive to the location of the indenter. Therefore, two loading conditions, viz. base and node indentations, are also considered. In the experiments, three geometric parameters (w_t, t_t, and θ_t shown in Fig.1b) for truss core were considered. In the parametric study, w_t is assumed to be equal to t_t to reduce the number of geometric parameters.

Two additional sandwich panels with double-sine corrugated (DSC) core and auxetic core, are simulated here. The double-sine corrugated (DSC) core was meshed by three-node shell elements (S3) as shown in Fig. 10(a). The appropriate mesh size was determined from a mesh convergency study. The double-sine corrugated core can be expressed by the following equation:

$$Y(x,z) = A \sin \frac{2\pi x}{\lambda} \sin \frac{2\pi z}{\lambda} \tag{1}$$

where, x and z axes are the two in-plane directions, and y-axis is the out-of-plane direction. A is the out-of-plane amplitude of the wave, which is 12.5 mm for all the panels. λ is the wavelength. Two full waves are introduced along the width of the panel (in the z-direction). The other geometric parameter is core thickness (t_d). Base and node indentations are also considered for the bending of double-sine corrugated

sandwich panel, shown schematically in Fig. 10(b).

The 3-D re-entrant auxetic core is shown in Fig. 10(c). The eight-node brick element (C3D8R) was employed to mesh the core. Mesh convergence study showed two elements along the thickness of each strut is sufficient to achieve a converged result. The geometric parameters of the auxetic core cell are the height of the vertical strut (h_a), the length of the re-entrant strut (l_a), the angle between the vertical strut and oblique strut (θ_a), and the edge length of the strut cross section (t_a). There is only one cell along the out-of-plane direction (y-direction) of the auxetic core. Therefore, the geometric parameters should satisfy the following relationship:

$$2h_a - 2l_a \cos \theta_a = h_c \tag{2}$$

where h_c is the core height and is 12.5 mm. Also, $h_a = 2l_a$ in the parametric study. Therefore, only two parameters, viz. θ_a and t_a, are varied. The geometric parameters of all the sandwich panels investigated in this section are listed in

Table 3 to 7.

(a)   (b)
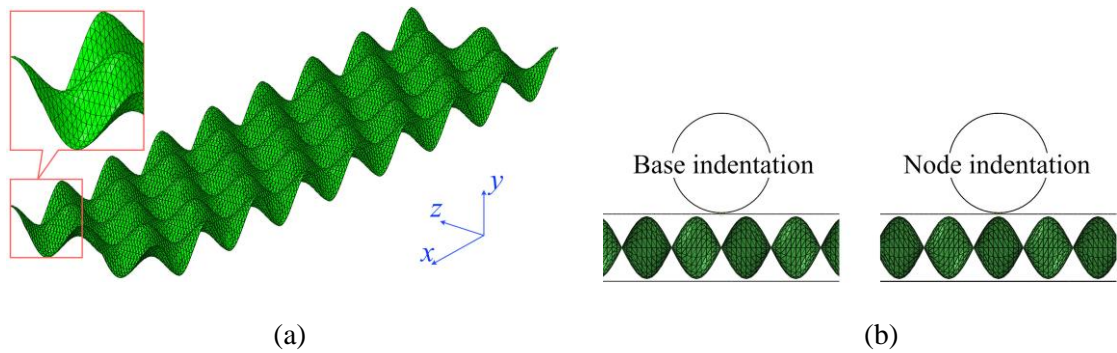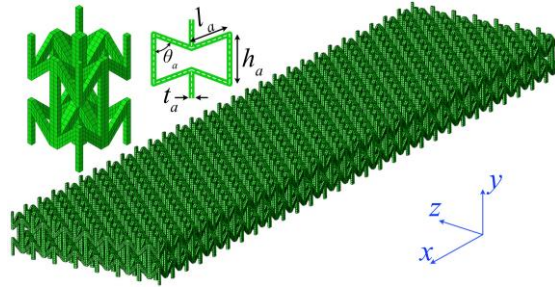
(c)

Fig. 10. Finite element model of the (a) double-sine corrugated core; (b) base indentation and node indentation of the panels with DSC core; (c) 3D re-entrant auxetic core.

Table 3. Geometric parameters of the sandwich panels with corrugated core

Sample	C-1	C-2	C-3	C-4	C-5	C-6	C-7	C-8	C-9
t_c (mm)	0.3	0.3	0.3	0.6	0.6	0.6	1.0	1.0	1.0
θ_c (°)	30	45	60	30	45	60	30	45	60

Table 4. Geometric parameters of the sandwich panels with truss core

Sample	T-1	T-2	T-3	T-4	T-5	T-6	T-7	T-8	T-9
w_t (mm)	0.3	0.3	0.3	0.6	0.6	0.6	1.0	1.0	1.0
θ_t (°)	22.2	35.3	50.8	22.2	35.3	50.8	22.2	35.3	50.8

Table 5. Geometric parameters of the sandwich panels with honeycomb core

Sample	H-1	H-2	H-3	H-4	H-5	H-6	H-7	H-8	H-9
d_h (mm)	3.18	3.18	3.18	3.97	3.97	3.97	6.35	6.35	6.35
t_h (mm)	0.0254	0.0381	0.0762	0.0254	0.0381	0.0762	0.0254	0.0381	0.0762

Table 6. Geometric parameters of the sandwich panels with DSC core

Sample	D-1	D-2	D-3	D-4	D-5	D-6

λ	15	15	20	20	25	25
t_d (mm)	0.25	0.5	0.25	0.5	0.25	0.5

Table 7. Geometric parameters of the sandwich panels with auxetic core

Sample	A-1	A-2	A-3	A-4	A-5	A-6
t_a (mm)	0.5	0.5	0.5	1.0	1.0	1.0
θ_a (°)	30	45	60	30	45	60

4.2.1 Corrugated core panels

Under longitudinal bending, the panel with a thinner core and smaller corrugation angle tends to have a larger indentation area. As shown in Fig. 11(a), the panel with $t_c = 0.3$ mm and $\theta_c = 30°$ (Panel C-1) has the widest and deepest indentation. Fig. 11(b) and (c) show two different types of load-displacement curves. The load in Fig. 11(b) decreases to a trough of approximately 0.46 kN after the first load (0.77 kN), then increases to a plateau of approximately 0.5 kN. The first load drop is triggered by bending of core webs, and the subsequent increase after the trough is due to the contact between the core webs and the top face-sheet. Beyond that, traveling hinges appear on every core web, and the load remains relatively constant. By contrast, for panel C-8, the load decreases almost monotonically (with slight fluctuations) after the first peak (3.02 kN). The core webs are relatively stronger in this panel (due to a higher t_c and θ_c). The load drop occurs when the top face-sheet bends and continues with the bending of the core webs afterwards. At the same time, the bottom face-sheet also bends, which also contribute to the load drop.
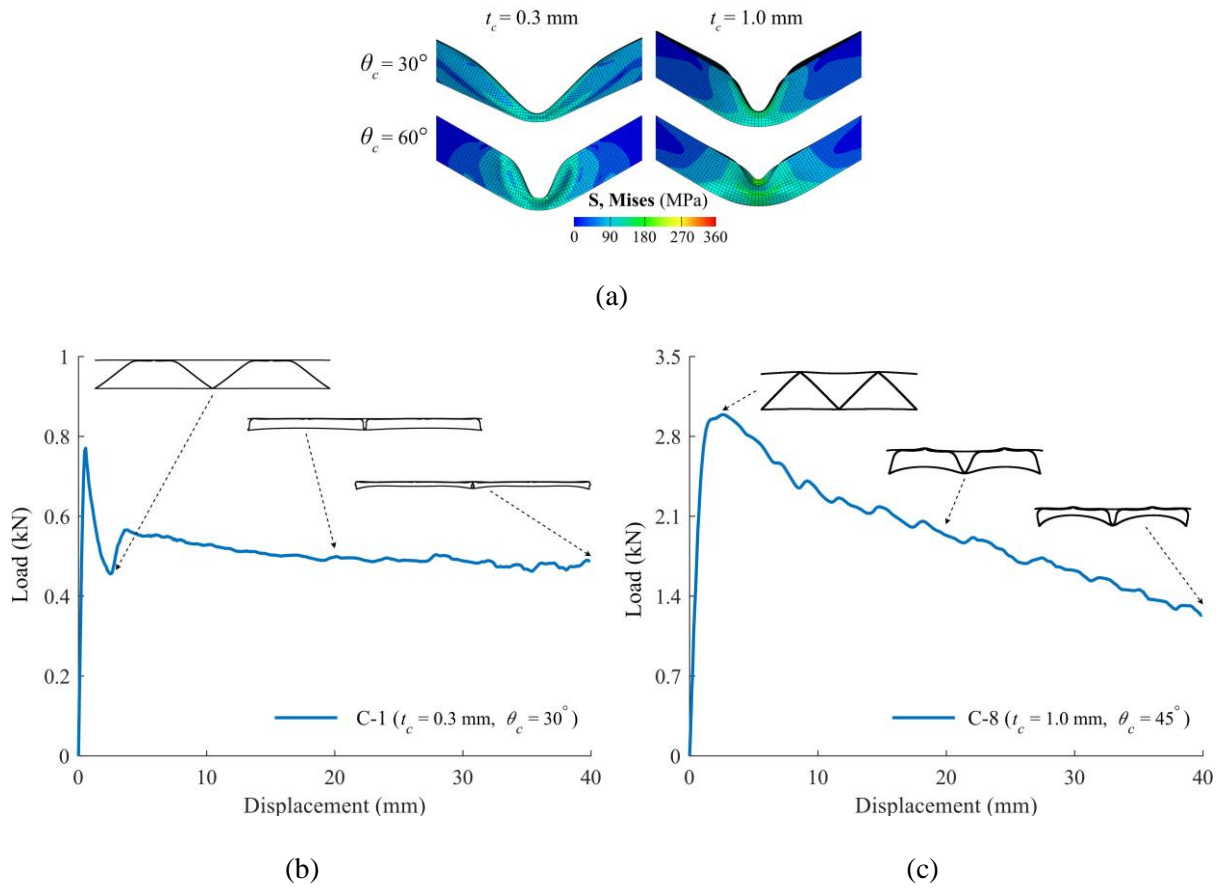
Fig. 11. Corrugated core panels under longitudinal bending: (a) t_c = 0.3 mm, 0.6 mm, and θ_c = 30°, 60°; (b) load-displacement curves for panels C-1, and (c) C-8.

Under node indentation, a corrugated panel with a thinner core (such as panel C-2) also experienced global uniaxial crushing during transverse bending as shown in Fig. 12(a). By contrast, the deformation in a panel with a thicker core (such as panel C-8) is localised to one side of the indenter as shown in Fig. 12 (b). For base indentation, the deformation of the panel is localised under the indenter, and the thinner core has a smaller indentation area. The peak load of the panel under node indentation is higher than that in base indentation. For example, for panel C-2, the peak load in node and base indentations are 0.72 kN and 0.46 kN, respectively. For panel C-8, the peak load under node indentation (2.42 kN) is almost five times higher than in base indentation (0.50 kN). The fluctuations in the load-displacement curve for

the panel C-2 under node indentation - see Fig. 12(a) - is due to progressive deformation of corrugated core that extends outwards from the base of the indenter.

(a)   (b)
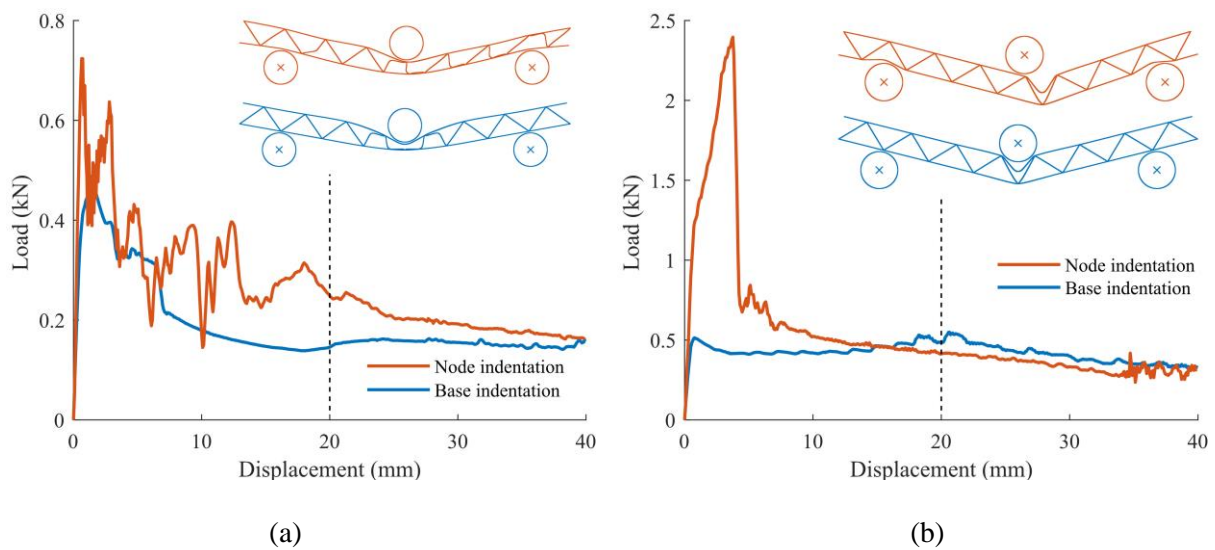
Fig. 12. Load-displacement curves from transverse bending of panels (a) C-2 and (b) C-8. All deformed plots shown correspond to an indenter displacement of 20 mm.

4.2.2 Truss core panels

Two deformation modes (Mode TI and TII) are observed for the truss core panel. In Mode TI, only the core cells under the indenter collapse (four struts of a cell bend) in both node and base indentations as shown in Fig. 13(a). In Mode TII, most of the core cells collapse as shown in Fig. 13(b). Correspondingly, the load-displacement curves of panels also display two different trends. However, the load fluctuates severely due to the progressive collapse of the core cells when the panel is deforming in Mode TII. Figure 13(a) shows that the peak load for node indentation (0.60 kN) is approximately 30% higher than that in base indentation (0.46 kN), because the indenter locates in a stronger place in node indentation. Fig. 13(c) shows that, in general, a panel with a thinner core cell strut and a smaller θ_t tends to deform in Mode TII.
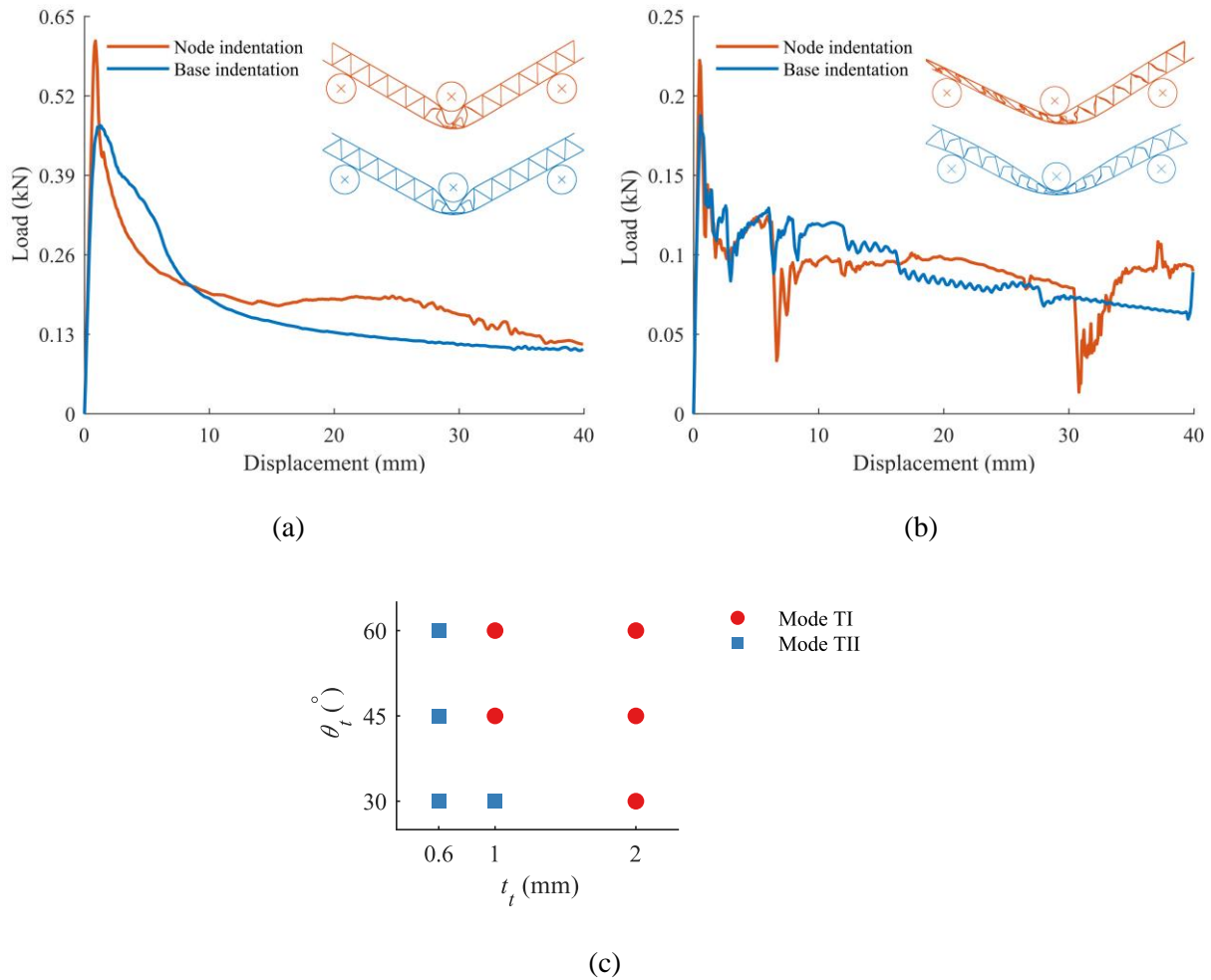
24

Fig. 13. Tuss core panels: (a) load-displacement curves of a panel deforming in Mode TI (panel T-9); (b) load-displacement curves of a panel deforming in Mode TII (panel T-6); (c) deformation modes and geometric parameters. The deformed plots in (a) and (b) correspond to an indenter displacement of 20 mm.

4.2.3 Honeycomb core panels

The deformation of all the honeycomb sandwich panels investigated here is identical to that observed in experiments – the face-sheet intrudes into the core under the indenter. As shown in Fig. 14(a), a thicker honeycomb wall thickness and a smaller cell size result in more localised indentation. The load-displacement curves also have a very similar trend to those in

the experiments (in Fig. 8). Therefore, only one curve, which is for the panel H-1, is shown here in Fig. 14(b).
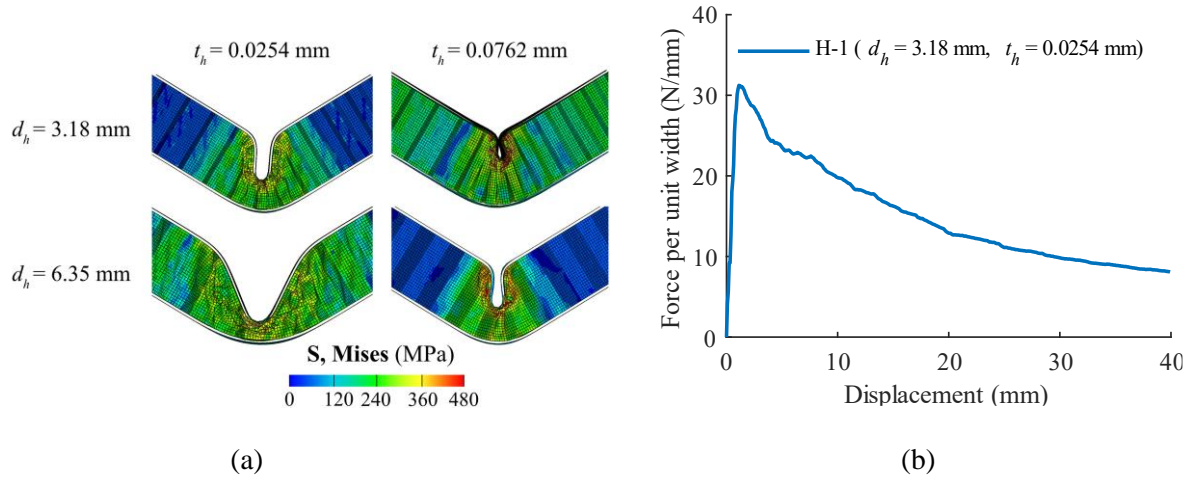

Fig. 14. Honeycomb core panels: (a) deformation of the panels with d_h = 3.18 mm, 6.35 mm, and t_h = 0.0254 mm, 0.0762 mm; (b) load-displacement curve of the panel H-1.

4.2.4 Double-sine corrugated (DSC) core panels

Six panels with three different λ and two different t_d were simulated. The deformation and load-displacement curves of the panels are shown in Fig. 15. In general, the deformation of the panels is similar to the panel described in the previous sections (4.2.1 to 4.2.3) – the core underneath the indenter, and in its vicinity, is crushed by the intrusion of the top face-sheet. A smaller t_d and a greater λ result in a greater extent of localised indentation. The differences in the deformation mode and load-displacement curve between base and node indentations are minor, except for panel D-6. The relatively stronger core and larger core wavelength of this panel lead to wrinkling of its top face-sheet under node indentation, leading to a significant increase in the load when the indenter displacement is beyond 18 mm, as shown in Fig. 15 (e). The load-displacement curves of other panels have a similar trend, i.e., increase rapidly to the peak and then decrease monotonically. For a smaller λ, the differences (both deformation mode and load-displacement curve) between the base and node indentation become less discernible.
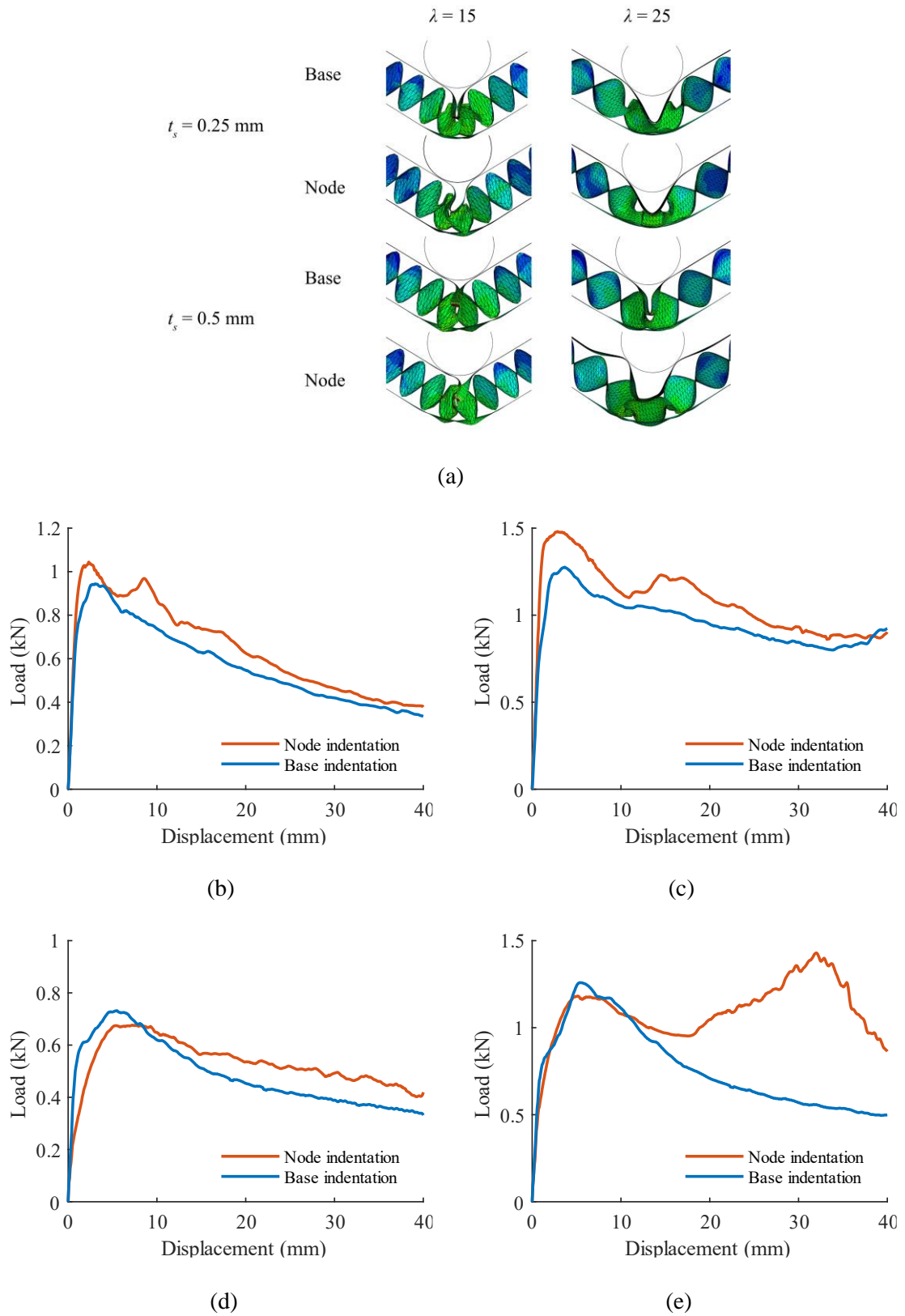
26

Fig. 15. DSC core panels: (a) deformation of panels with $\lambda = 15$, 25, and $t_d = 0.25$ mm, 0.5 mm; and, load-displacement curves for panels with panels (b) D-1; (c) D-5; (d D-2; (e) D-6.

4.2.5 3D re-entrant auxetic core panels

The 3D re-entrant auxetic core panels display different modes of deformation to those in previous sections (4.2.1 to 4.2.4), see Fig. 16. For panels with thin core struts, say, $t_a = 0.5$ mm, local indentation does not occur. The struts along y-direction bend, and the low shear strength of the core gives rise to relative motion between the two face-sheets in the x-direction. There is a relative displacement between face-sheets due to this relative motion. This mode of deformation mode is denoted as Mode AI. As the thickness of the core struts increases, say, to 1 mm, the thicker struts bend less due to an increase of its flexural rigidity, and the relative displacement between the two face-sheets is also smaller compared to the panel where $t_a = 0.5$ mm. Moreover, the local indentation becomes more evident when t_a increases from 0.5 mm to 1 mm. The core struts under the indenter get closer to each other along both the x and y directions due to the negative Poisson's ratio of the 3D re-entrant auxetic core. This deformation mode is denoted as Mode AII. By contrast, θ_a has little effect on the mode of deformation that develops. The load-displacement curves are also different from those of previous sub-sections. The panels with the same t_a of 0.5 mm but different θ_a exhibit an identical curve trend – the load slowly increases and remains almost constant. When t_a increases to 1.0 mm, the curves show different trends in the panels with different θ_a. Loads of the panels with $\theta_a = 30°$ and $60°$ both rapidly increase firstly, followed by a moderate increase to the peak. At this point, the top face-sheet starts to intrude into the core, which causes the drop of the load. However, beyond the indenter displacement of 25 mm, the load of the panel with $\theta_a = 60°$ starts to rise again, which is because the core with a larger θ_a is denser and the core struts under the indenter come into contact with each other at the indenter displacement of 25 mm.
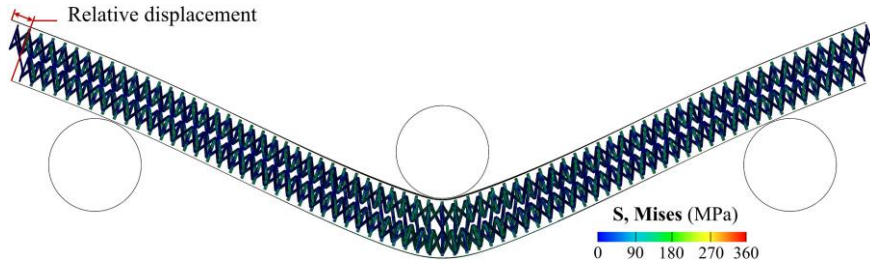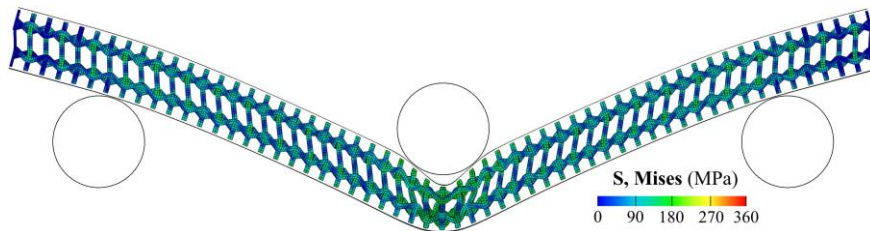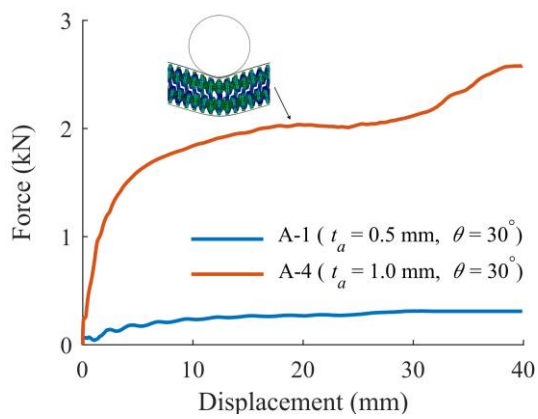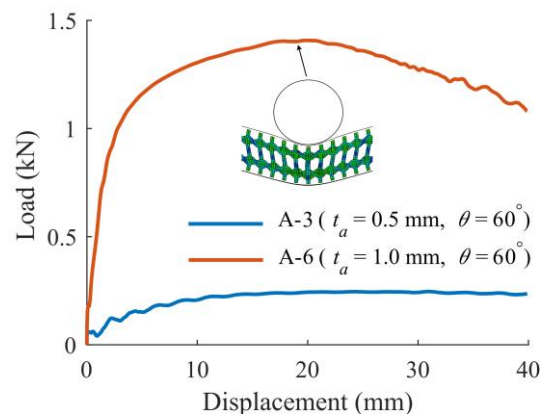
(a)
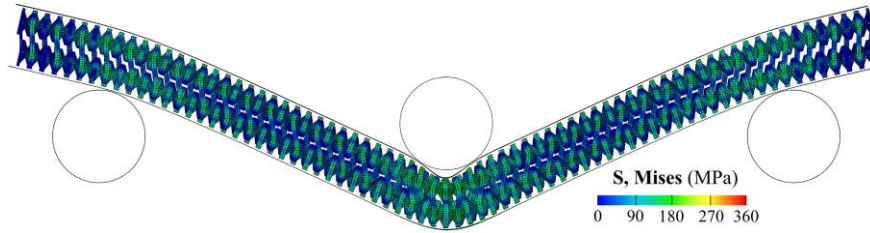
(b)
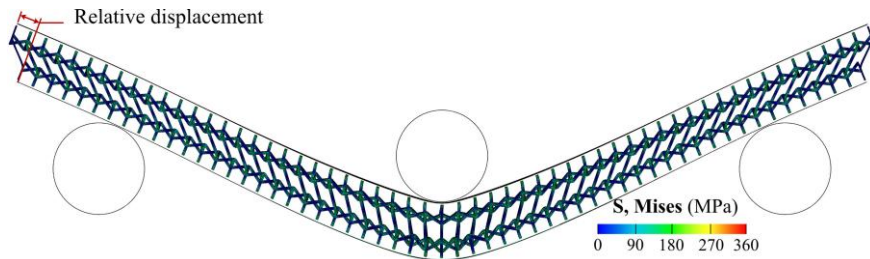
(c)

(d)

(e)

(f)

Fig. 16. Auxetic sandwich panel: deformation of panels (a) A-1 (Mode AI); (b) A-4 (Mode AII); (c) A-3 (Mode AI); (d) A-6 (Mode AII); and, load-displacement curves for panels (e) A-1 and A-4; (f) A-3 and A-6. The deformed plots in (e) and (f) correspond to an indenter displacement of 20 mm.

4.2.6 Comparison between sandwich panels

Three distinct modes of deformation were observed in the panels that were investigated. The first mode is the most common one, in which, both global bending and local indentation occur (e.g., Fig. 11a). Plastic hinges form in the middle of the top face-sheet, which significantly compressed the core under it. The load increases to the peak before dropping dramatically corresponding to bending of core cells; after that, it either decreases further or stabilises to a plateau value (e.g., Fig. 11 b and c). In the second mode, the core of the panel experiences global bending along with overall uniaxial crushing. This mode of deformation is more commonly observed in corrugated and truss sandwich panel with lower density cores (e.g., Fig. 13b). Loads of panels deformed in this mode fluctuate severely (e.g., Fig. 13b). The third mode is only observed in auxetic sandwich panels where the panel undergoes global bending with no localised indentation beneath the indenter (Fig. 16a). Here, the load rises rapidly towards a plateau such as in Fig. 16(e).

To assess the energy absorption ability of the different panels, their specific energy absorption (SEA) – this is defined as the energy absorbed per unit mass of the panel - is calculated. The absorbed energy is the area under the load-displacement curve between the indenter displacement of 0 to 40 mm. In the calculation of the SEA, only the mass of the panel between the supports is taken into account. The relative density (RD) of the cores can be expressed as:

Corrugated core: $\quad RD = \dfrac{t_c}{h_c \cos \theta_c}$ $\hfill$ (3)

Truss core: $$RD = \frac{2t_t^2 \sin\theta_t}{h_c^2 \cos^4\theta_t} \tag{4}$$

Honeycomb core: $$RD = \frac{2t_h}{d_h} \tag{5}$$

DSC core:
$$
\begin{aligned}
RD &= \frac{t_d}{2\lambda l}\int_0^{2\lambda}\int_0^l \sqrt{\frac{4A^2\pi^2}{\lambda^2}\left(\sin^2\frac{2\pi x}{\lambda}\cos^2\frac{2\pi y}{\lambda} + \cos^2\frac{2\pi x}{\lambda}\sin^2\frac{2\pi y}{\lambda}\right) + 1}\, dx dy
\end{aligned}
\tag{6}
$$

Auxetic core: $$RD = \frac{4l_a t_a^2 + h_a t_a^2}{2l_a^2 \sin^2\theta_a (h_a - l_a\cos\theta)} \tag{7}$$
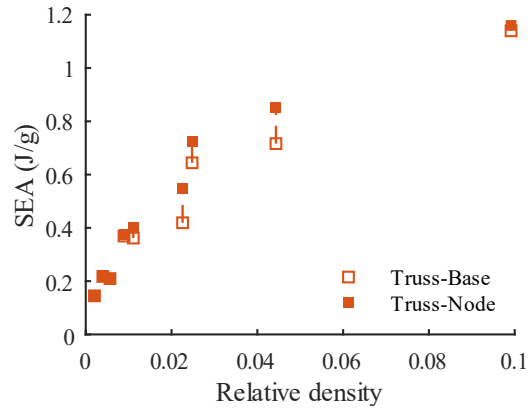
Fig. 17 shows the SEA vs. relative density of all sandwich panel cores in the parametric study. For all the panels studied, a panel with higher core relative density tends to have a greater SEA. The SEA of corrugated sandwich panel increases with the relative density of corrugated sandwich panel. However, the increase in SEA with the relative density is not monolithic, which is due to the different deformation mode of the panels asdetailed inin our previous papers [36, 37]. On the other hand, the SEA of truss sandwich panels increases monolithically with the increase of the core relative density. Moreover, as shown in Fig. 17 (c), the DSC core sandwich panel with lower λ and higher t_d has greater SEA. Furthermore, for auxetic sandwich panel, a larger t_a results in a greater SEA. However, when t_a is the same, the panel with the θ_a of 45° has the lowest SEA.

When comparing the performance of the panels with identical core relative density, the panel with a honeycomb core has the highest SEA. The panels with corrugated core under transverse bending and auxetic core exhibit the lowest SEA. However, the SEA of the panels with corrugated core under longitudinal bending and DSC core is similar. Although the auxetic sandwich panel has a relatively low SEA, the load-displacement curve display a desirable shape for energy absorption (i.e., no presence of a pronounced peak load and a long plateau with a relatively constant load). Figure 17 also shows that the SEA of the corrugated, truss, and DSC core panels depends on whether the panel is under base or node indentation. In general, the
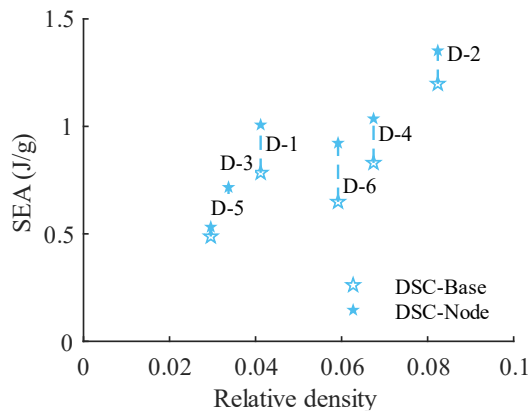
SEA of panels under node indention is higher than that of panels under base indentation. In addition, the SEA of a corrugated core panel is higher under longitudinal bending compared to that of the panel under transverse bending. This difference becomes greater with the increase of relative density.
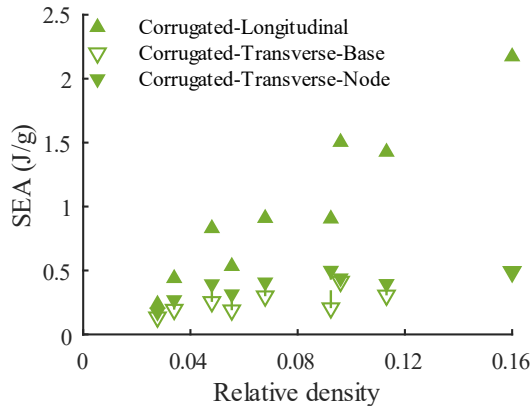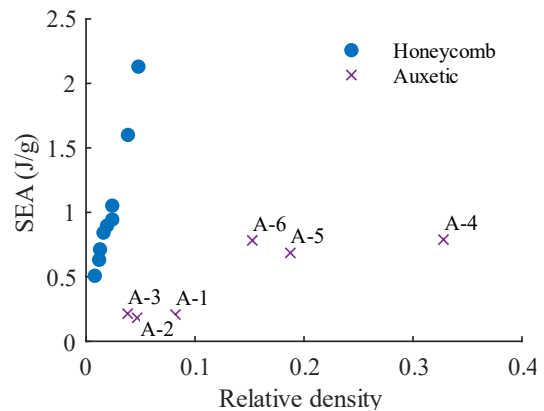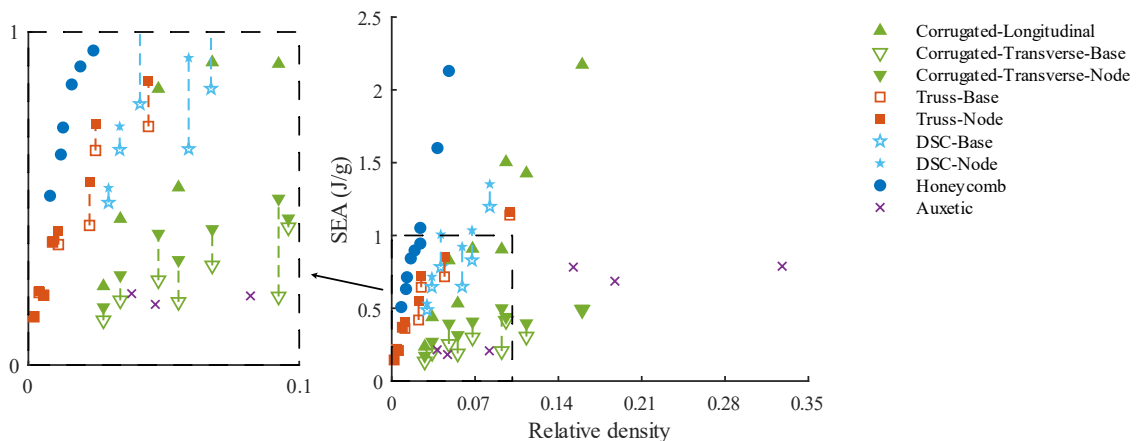

(a)

(b)

(c)

(d)

(e)

Fig. 17. SEA *vs*. relative density of the (a) corrugated, (b) truss, (c) DSC, (d) honeycomb and auxetic cores, and (e) is the comparison for all core types.

5. CONCLUSIONS

Three-point bending performance of sandwich panels with triangular corrugated core, pyramidal truss core, honeycomb core, aluminum foam core, double sine corrugated core (DSC), and 3D re-entrant auxetic core was studied and compared. Experiments were firstly conducted on the corrugated, truss, honeycomb, and foam core sandwich panels. Most of the panels experienced global bending and local indentation. Subsequently, parametric study was performed using the validates numerical models. The DSC and auxetic sandwich panels along with the panels in experiments except for foam sandwich panel were included in the parametric study. Three deformation modes and load-displacement trends were observed. In all types of sandwich panels, the SEA tended to increase with the increase of the relative density of the core. Within the range of parameters studied, when the relative density was the same, honeycomb sandwich panel had the greatest SEA, and the panel with corrugated (transverse loading) and auxetic core had the lowest SEA.

REFERENCES

[1]   C.E. Harris, J.H. Starnes, M.J. Shuart, An assessment of the state-of-the-art in the design and manufacturing of large composite structures for aerospace vehicles, NASA Tech. Memo. 39 (2001) 1–24.

[2]   B. Metschkow, Sandwich panels in shipbuilding, Polish Marit. Res. (2006) 5–8.

[3]   A. Wahrhaftig, H. Ribeiro, A. Nascimento, M. Filho, Analysis of a new composite material for watercraft manufacturing, J. Mar. Sci. Appl. 15 (2016) 336–342.

[4]   J.S. Kim, S.J. Lee, K.B. Shin, Manufacturing and structural safety evaluation of a composite train carbody, Compos. Struct. 78 (2007) 468–476.

[5]   F. Zhu, G. Lu, D. Ruan, Z. Wang, Plastic Deformation, Failure and Energy Absorption of Sandwich Structures with Metallic Cellular Cores, Int. J. Prot. Struct. 1 (2010) 507–541.

[6]   L.J. Gibson, Cellular solids, MRS Bull. 28 (2003) 270–274.

[7]   T.M. McCormack, R. Miller, O. Kesler, L.J. Gibson, Failure of sandwich beams with metallic foam cores, Int. J. Solids Struct. 38 (2001) 4901–4920.

[8]   V. Crupi, R. Montanini, Aluminium foam sandwiches collapse modes under static and dynamic three-point bending, Int. J. Impact Eng. 34 (2007) 509–521.

[9]   S. Xu, D. Ruan, G. Lu, Strength enhancement of aluminium foams and honeycombs by entrapped air under dynamic loadings. Int. J. Impact Eng. 74 (2014) 120–125.

[10]   M.A. Khan, A.K. Syed, H. Ijaz, R.M.B.R. Shah, Experimental and numerical analysis of flexural and impact behaviour of glass/pp sandwich panel for automotive structural applications, Adv. Compos. Mater. 3046 (2017) 1–20.

[11]   K.P. Dharmasena, H.N.G. Wadley, Z. Xue, J.W. Hutchinson, Mechanical response of metallic honeycomb sandwich panel structures to high-intensity dynamic loading, Int. J. Impact Eng. 35 (2008) 1063–1074.

[12] H. Ebrahimi, R. Ghosh, E. Mahdi, H. Nayeb-Hashemi, A. Vaziri, Honeycomb sandwich panels subjected to combined shock and projectile impact, Int. J. Impact Eng. 95 (2016) 1–11.

[13] L. Wahl, S. Maas, D. Waldmann, A. Zürbes, P. Frères, Shear stresses in honeycomb sandwich plates: Analytical solution, finite element method and experimental verification, J. Sandw. Struct. Mater. 14 (2012) 449–468.

[14] V.G.K. Menta, R.R. Vuppalapati, K. Chandrashekhara, D. Pfitzinger, N. Phan, Manufacturing and mechanical performance evaluation of resin-infused honeycomb composites, J. Reinf. Plast. Compos. 31 (2012) 415–423.

[15] V. Crupi, E. Kara, G. Epasto, E. Guglielmino, H. Aykul, Theoretical and experimental analysis for the impact response of glass fibre reinforced aluminium honeycomb sandwiches, J. Sandw. Struct. Mater. 20 (2018) 42–69.

[16] V. Crupi, G. Epasto, E. Guglielmino, Collapse modes in aluminium honeycomb sandwich panels under bending and impact loading, Int. J. Impact Eng. 43 (2012) 6–15.

[17] G. Sun, X. Huo, D. Chen, Q. Li, Experimental and numerical study on honeycomb sandwich panels under bending and in-panel compression, Mater. Des. 133 (2017) 154–168.

[18] G.W. Kooistra, D.T. Queheillalt, H.N.G. Wadley, Shear behavior of aluminum lattice truss sandwich panel structures, Mater. Sci. Eng. A. 472 (2008) 242–250.

[19] V.S. Deshpande, N.A. Fleck, Collapse of truss core sandwich beams in 3-point bending, Int. J. Solids Struct. 38 (2001) 6275–6305.

[20] J. Xiong, L. Ma, S. Pan, L. Wu, J. Papadopoulos, A. Vaziri, Shear and bending performance of carbon fiber composite sandwich panels with pyramidal truss cores, Acta Mater. 60 (2012) 1455–1466.

[21] N. Dahiwale, S. Panigrahi, K. Akella, Numerical analyses of sandwich panels with

triangular core subjected to impact loading, J. Sandw. Struct. Mater. 17 (2015) 238–257.

[22] P. Zhang, J. Liu, Y. Cheng, H. Hou, C. Wang, Y. Li, Dynamic response of metallic trapezoidal corrugated-core sandwich panels subjected to air blast loading - An experimental study, Mater. Des. 65 (2015) 221–230.

[23] X. Yang, J. Ma, Y. Shi, Y. Sun, J. Yang, Crashworthiness investigation of the bio-inspired bi-directionally corrugated core sandwich panel under quasi-static crushing load, Mater. Des. 135 (2017) 275–290.

[24] T. Boonkong, Y.O. Shen, Z.W. Guan, W.J. Cantwell, The low velocity impact response of curvilinear-core sandwich structures, Int. J. Impact Eng. 93 (2016) 28–38.

[25] F. Côté, V.S. Deshpande, N.A. Fleck, A.G. Evans, The compressive and shear responses of corrugated and diamond lattice materials, Int. J. Solids Struct. 43 (2006) 6220–6242.

[26] T.J. Lu, J.W. Hutchinson, A.G. Evans, Optimal design of a flexural actuator, J. Mech. Phys. Solids. 49 (2001) 2071–2093.

[27] L. Valdevit, J.W. Hutchinson, A.G. Evans, Structurally optimized sandwich panels with prismatic cores, Int. J. Solids Struct. 41 (2004) 5105–5124.

[28] L. Valdevit, Z. Wei, C. Mercer, F.W. Zok, A.G. Evans, Structural performance of near-optimal sandwich panels with corrugated cores, Int. J. Solids Struct. 43 (2006) 4888–4905.

[29] N.A. Yaraghi, N. Guarín-Zapata, L.K. Grunenfelder, E. Hintsala, S. Bhowmick, J.M. Hiller, M. Betts, E.L. Principe, J.Y. Jung, L. Sheppard, R. Wuhrer, J. McKittrick, P.D. Zavattieri, D. Kisailus, A Sinusoidally Architected Helicoidal Biocomposite, Adv. Mater. 28 (2016) 6835–6844.

[30] X. Yang, J. Ma, Y. Shi, Y. Sun, J. Yang, Crashworthiness investigation of the bio-inspired bi-directionally corrugated core sandwich panel under quasi-static crushing load, Mater. Des. 135 (2017) 275–290.

[31] X.T. Wang, B. Wang, X.W. Li, L. Ma, Mechanical properties of 3D re-entrant auxetic cellular structures, Int. J. Mech. Sci. 131–132 (2017) 396–407.

[32] L. Yang, O. Harrysson, H. West, D. Cormier, Mechanical properties of 3D re-entrant honeycomb auxetic structures realized via additive manufacturing, Int. J. Solids Struct. 69–70 (2015) 475–490.

[33] G. Chen, P. Zhang, N. Deng, S. Cai, Y. Cheng, J. Liu, Paper tube-guided blast response of sandwich panels with auxetic re-entrant and regular hexagonal honeycomb cores–An experimental study, Eng. Struct. 253 (2022) 113790.

[34] M.A. Yahaya, D. Ruan, G. Lu, M.S. Dargusch. Response of aluminium honeycomb sandwich panels subjected to foam projectile impact–An experimental study. Int. J. Impact Eng. 75 (2015) 100–9.

[35] V. Crupi, G. Epasto, E. Guglielmino, H. Mozafari, S. Najafian, Computed tomography-based reconstruction and finite element modelling of honeycomb sandwiches under low-velocity impacts. J. Sandw. Struct. Mater. 16 (2014) 377–97.

[36] F. Xia, T.X. Yu, Y. Durandet, D. Ruan, Triangular corrugated sandwich panels under longitudinal bending. Thin-Walled Struct. 169 (2021):108359.

[37] F. Xia, Y. Durandet, T.X. Yu, D. Ruan, Large deformation of corrugated sandwich panels under three-point bending, J. Sandw. Struct. Mater. 23 (2020) 3336–67.